

Frustrated spin models on two- and three-dimensional decorated lattices with high residual entropy

D. V. Dmitriev,* V. Ya. Krivnov, and O. A. Vasilyev

Institute of Biochemical Physics of RAS,

Kosygin str. 4, 119334, Moscow, Russia.

(Dated:)

We study the ground-state properties of a family of frustrated spin-1/2 Heisenberg models on two- and three-dimensional decorated lattices composed of connected star-shaped units. Each star is built from edge-sharing triangles with an antiferromagnetic interaction on the shared side and ferromagnetic interactions on the others. At a critical coupling ratio, the ideal star model - defined by equal ferromagnetic interactions - exhibits a macroscopically degenerate ground state, which we map onto a site percolation problem on the Lieb lattice. This mapping enables the calculation of exponential ground-state degeneracy and the corresponding residual entropy for square, triangular, honeycomb, and cubic lattices. Remarkably, the residual entropy remains high for all studied lattices, exceeding 60% of the maximal value $\ln(2)$. Despite a gapless quadratic one-magnon spectrum, the low-temperature thermodynamics is governed by exponentially numerous gapped excitations. For a distorted-star variant of the model, the ground-state manifold is equivalent to that of decoupled ferromagnetic clusters, leading to exponential degeneracy with a lower, yet still substantial, residual entropy. At low temperature the system mimics a paramagnetic crystal of non-interacting spins with high spin value ($s = 4$ for a square lattice). The obtained results establish a structural design principle for engineering quantum magnets with a high ground-state degeneracy, suggesting promising candidates for enhanced magnetocaloric cooling and quantum thermal machines.

* dmitriev@deom.chph.ras.ru

I. INTRODUCTION

Quantum magnets on geometrically frustrated lattices often host macroscopically degenerate ground states, a phenomenon closely tied to flat, dispersionless magnon bands [1–3]. This flat-band physics, highlighted in seminal studies of highly frustrated antiferromagnets [4, 5], arises from localized magnon states confined to specific lattice cells by destructive interference [6]. These localized states can be combined into exact multi-magnon eigenstates, enabling a mapping to a classical lattice gas model [5, 7, 8]. Such degeneracy leads to distinctive thermodynamic features like magnetization plateaus and enhanced magnetocaloric effects [5, 6, 9–11].

A distinct route to high degeneracy emerges in systems with competing ferromagnetic (F) and antiferromagnetic (AF) interactions. At a quantum critical point where different phases meet, these F-AF models, such as the frustrated delta-chain and its extensions [12–19], exhibit macroscopic degeneracy and high residual entropy even at zero field - a property relevant for magnetic cooling applications. Beyond adiabatic demagnetization, such macroscopic degeneracy at a quantum critical point is also central to the operation of quantum thermal machines. Enhanced work output and efficiency can be achieved when a thermodynamic cycle is operated across a quantum critical point, utilizing the large ground-state degeneracy g_{\max} as an 'entropic lever'. The maximal net work extractable scales as $W = k_B (T_{\max} - T_{\min}) \ln (g_{\max})$, directly linking the performance of the machine to the extensive degeneracy of the model [20–22].

Recent work has extended this framework to models built from diamond-shaped clusters. A spin- $\frac{1}{2}$ chain of distorted diamonds was shown to host flat bands for one-, two-, and three-magnon states [23]. Similarly, models on diamond-decorated square and cubic lattices support up to five or seven localized magnons per cell [24]. The inclusion of these multi-magnon states substantially amplifies ground-state degeneracy. Experimentally, diamond units with competing F and AF interactions are realized in materials such as $K_3Cu_3AlO_2(SO_4)_4$ [25] and $K_2Cu_3(MoO_4)_4$ [26].

Purely antiferromagnetic models of ideal diamonds also exhibit rich physics, with phases including macroscopically degenerate monomer-dimer states [27–30]. However, a different degeneracy mechanism operates in F-AF models with ideal diamonds at a special coupling ratio. Here, the ground state factorizes into decoupled clusters with identical energy per

spin, leading to exponential degeneracy from isolated ferromagnetic clusters embedded in a singlet background [23, 24].

In this work, we explore a structural variant of these models: lattices constructed from connected star units rather than conventional bond decorations. We demonstrate that this architecture sustains exceptionally high and robust residual entropy across various two- and three-dimensional lattices, highlighting its potential as a design principle for high-entropy quantum magnets and, consequently, for applications in efficient cooling and quantum thermal machines.

The remainder of this paper is organized as follows. In Section II, we introduce the two- and three-dimensional lattices constructed from edge-sharing triangular units. We demonstrate that the Hamiltonian for so constructed models maps onto a Lieb lattice, with composite spins $L = 0$ (singlet) or $L = 1$ (triplet) occupying its sites. This mapping allows us to calculate the exponential ground-state degeneracy and residual entropy via a connection to a classical site percolation problem. Section III explores the same models with distorted unit blocks, analyzing how this modification influences the ground-state degeneracy and residual entropy. Finally, in Section IV, we summarize our key findings.

II. IDEAL STAR MODEL ON THE 2D AND 3D LATTICES

In our previous work [24], we introduced an extension of the diamond chain model with high ground state degeneracy [23] to two- and three-dimensional diamond-decorated lattices. Here, we consider an alternative structural variant, in which the diamond diagonals occupy the lattice sites, rather than the central spins used in [24]. Figure 1 compares these two extensions for the square lattice: panel (a) shows the diamond-decorated lattice studied in [24], while panel (b) illustrates the present alternative construction. Although we explicitly formulate the extension for a square lattice, the analysis and results are fully general and apply to any two- or three-dimensional lattice.

As shown in Fig. 1b, the square lattice is constructed from connected elementary cells, or stars. A single star is illustrated in Fig. 2. It consists of edge-sharing triangles with an antiferromagnetic exchange J_1 (red) on the shared side and equal ferromagnetic exchanges J_2 (black) on the remaining sides. In the following, we refer to the spins on the diagonal as dimer spins and the outer spins as monomer spins.

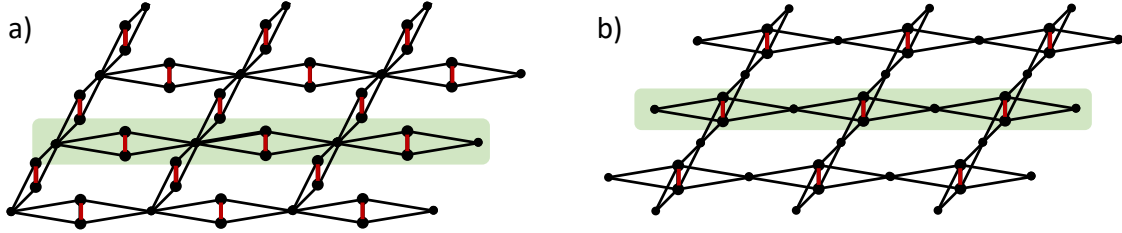


FIG. 1. Two versions of the extension of the diamond chain (shaded) to the square lattice: a) the diamond-decorated square lattice, and b) the square lattice formed by connected stars.

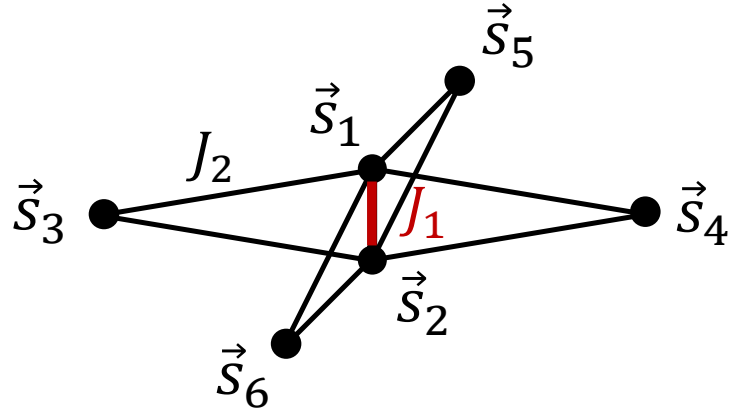


FIG. 2. An elementary cell (star) for the square lattice.

The total Hamiltonian is a sum over all local star Hamiltonians:

$$\hat{H} = \sum_i \hat{H}_i \quad (1)$$

The local Hamiltonian for the single star shown in Fig.2 has the form

$$\hat{H}_0 = J_1 \mathbf{s}_1 \cdot \mathbf{s}_2 - J_2 (\mathbf{s}_1 + \mathbf{s}_2) \cdot (\mathbf{s}_3 + \mathbf{s}_4 + \mathbf{s}_5 + \mathbf{s}_6) + \frac{3}{4} J_1 \quad (2)$$

where \mathbf{s}_i are spin- $\frac{1}{2}$ operators and the constant in (1) is added for convenience, it ensures the ground state energy of the singlet sector is zero.

As follows from Hamiltonian (2), there is a local conservation of a composite spin $\mathbf{L} = \mathbf{s}_1 + \mathbf{s}_2$ on the diagonal of the star (dimer). Composite spin is a conserved quantity with a quantum spin number $L = 0$ or $L = 1$, which corresponds to the singlet or triplet state of the dimer, respectively. The singlet state of the dimer shown in Fig.2, $(s_1^- - s_2^-) |F\rangle$ (where $|F\rangle$ is the fully polarized state with all spins down), is an exact state of \hat{H}_0 , independent

of the configuration of the monomer spins $\mathbf{s}_3, \mathbf{s}_4, \mathbf{s}_5, \mathbf{s}_6$. In terms of the composite spin, the local Hamiltonian (2) simplifies to

$$\hat{H}_0 = \frac{J_1}{2} \mathbf{L}^2 - J_2 \mathbf{L} \cdot (\mathbf{s}_3 + \mathbf{s}_4 + \mathbf{s}_5 + \mathbf{s}_6) \quad (3)$$

The ground state of (3) depends on the relation between the exchanges J_1 and J_2 . For $J_1 < 2J_2$, the ferromagnetic state with $L = 1$ and the total spin $S_{tot} = 3$ is the ground state of \hat{H}_0 , with the energy $E_F = J_1 - 2J_2$. For $J_1 > 2J_2$, the ground state of \hat{H}_0 is degenerate and has $L = 0$, which means that the four monomer spins $\mathbf{s}_3, \dots, \mathbf{s}_6$ are effectively free. This yields a local ground-state manifold composed of one quintet ($S_{tot} = 2$), three triplets ($S_{tot} = 1$), and two singlets ($S_{tot} = 0$), all with energy $E_0 = 0$.

Therefore, the global ground state phase diagram of model (1) consists of the ferromagnetic (F) for $J_1 < 2J_2$ and monomer-dimer (MD) phases for $J_1 > 2J_2$. The F phase, with all $L_i = 1$, has a degeneracy of $(\mathcal{N}+1)$, where \mathcal{N} is the total number of spins in the system. The monomer-dimer (MD) phase, with all $L_i = 0$, has a macroscopic ground state degeneracy of $2^{N_{bond}}$, where N_{bond} is the number of free monomer spins $\mathbf{s}_{i,j}$ located on the bonds between the sites \mathbf{i} and \mathbf{j} .

At the quantum critical point $J_1 = 2J_2$, the ferromagnetic state of local Hamiltonian (3) with $L = 1$ and $S_{tot} = 3$ becomes degenerate with the $L = 0$ ground state manifold. This additional degeneracy of the local Hamiltonian at $J_1 = 2J_2$ induces a significantly higher ground state degeneracy of the total system. In this work, we focus on this quantum critical point, which separates the F and MD phases. For convenience, we set the energy scale with $J_2 = 1$ and take $J_1 = 2$.

Consequently, the local Hamiltonians $\hat{H}_{\mathbf{i}}$ in (1) centered at site $\mathbf{i} = (i_x, i_y)$ of the square lattice can be expressed as

$$\hat{H}_{\mathbf{i}} = \mathbf{L}_{\mathbf{i}}^2 - \sum_{\mathbf{j}} \mathbf{L}_{\mathbf{i}} \cdot \mathbf{s}_{\mathbf{i},\mathbf{j}} \quad (4)$$

where $\mathbf{s}_{\mathbf{i},\mathbf{j}}$ are spin- $\frac{1}{2}$ operators on the bonds between sites \mathbf{i} and \mathbf{j} . As illustrated in Fig.3, the original spin- $\frac{1}{2}$ system maps onto a Lieb lattice: the monomer spins $\mathbf{s}_{\mathbf{i},\mathbf{j}}$ reside on bonds, and the composite spins $\mathbf{L}_{\mathbf{i}}$ occupy the sites of the Lieb lattice.

For an arbitrary lattice with coordination number z , the general Hamiltonian can be written in the form

$$\hat{H} = \frac{z}{4} \sum_{\mathbf{i}} \mathbf{L}_{\mathbf{i}}^2 - \sum_{\langle \mathbf{i},\mathbf{j} \rangle} (\mathbf{L}_{\mathbf{i}} + \mathbf{L}_{\mathbf{j}}) \cdot \mathbf{s}_{\mathbf{i},\mathbf{j}} \quad (5)$$

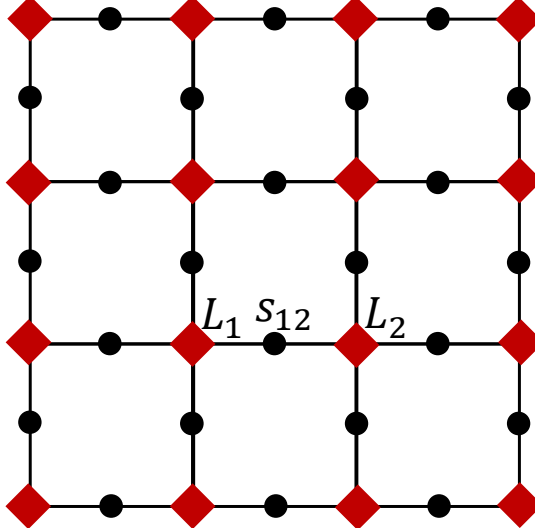


FIG. 3. Mapping of the model to a square Lieb lattice. Sites host composite spins \mathbf{L}_i ; bonds host monomer spins- $\frac{1}{2}$, $\mathbf{s}_{i,j}$.

where the second sum runs over all nearest-neighbor sites \mathbf{i} and \mathbf{j} on the corresponding lattice.

A. Ground state degeneracy

A singlet state of a dimer at site \mathbf{i} ($L_i = 0$) effectively decouples the neighboring bond spins $\mathbf{s}_{i,j}$. Therefore it is more convenient to compute the ground state degeneracy not in terms of magnon sectors (or the total S^z), but by enumerating all possible configurations of such singlet sites on the Lieb lattice. Each ground state is uniquely associated with a specific configuration of singlet sites; the total degeneracy is obtained by summing contributions from every such configuration.

Thus, the problem maps exactly onto a *site percolation problem on the Lieb lattice*, where sites in the triplet state ($L_i = 1$) are considered ‘connected’ and singlet sites ($L_i = 0$) are ‘disconnected’. The calculation follows the procedure of Ref.[24], which addressed a *bond percolation* problem for diamond-decorated lattices; here we adapt it to site percolation.

For a particular configuration ω_K with K connected sites (triplet states), the lattice effectively decomposes into disconnected ferromagnetic clusters. For the i -th cluster containing n_i connected sites and l_i bonds, the total number of spins- $\frac{1}{2}$ is $(2n_i + l_i)$, yielding a cluster

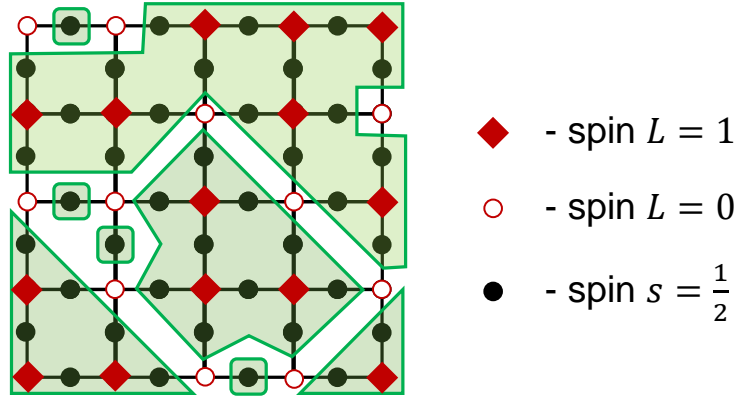


FIG. 4. A 4×4 Lieb lattice with a specific configuration of singlet sites (open circles, $L_i = 0$). Shaded regions denote the resulting ferromagnetic clusters.

degeneracy $(2n_i + l_i + 1)$ (all possible S^z projections of ferromagnetic ground state). The total degeneracy for configuration ω_K is the product of the numbers of ground states over all clusters

$$W(\omega_K, N) = \prod_{i \in \omega_K} (2n_i + l_i + 1) \quad (6)$$

As an illustration, Fig.4 shows a specific configuration of ‘connected’ sites on 4×4 square lattice with open boundaries. In this configuration, eight distinct clusters emerge: four single-spin clusters and clusters containing 4, 12, 16, 32 spins- $\frac{1}{2}$. According to Eq.(6), the ground state degeneracy for this particular configuration is $W = 2^4 \cdot 5 \cdot 13 \cdot 17 \cdot 33 = 583440$ states.

The total degeneracy for a fixed number K of connected sites on an N -site lattice is obtained by summing over all possible configurations ω_K

$$W(K, N) = \sum_{\omega_K} W(\omega_K, N) \quad (7)$$

Figure 5(a)–(d) plots $\ln W(K, N)$ versus the fraction of connected sites $p = K/N$. For all lattices, $W(K, N)$ peaks well below the corresponding site-percolation threshold p_c (red vertical lines), at approximately $p_0 \simeq 0.3$ (hexagonal), $p_0 \simeq 0.2$ (square), $p_0 \simeq 0.1$ (triangular and cubic) lattices. Below p_c , the system consists of many small clusters whose number scales with N , leading to exponential scaling $W \sim \exp(\text{const} \cdot N)$. Above p_c , a single infinite ferromagnetic cluster dominates, and W scales only linearly with N . Since $p_0 < p_c$ for all studied lattices, the dominant contributions to the total degeneracy come from configurations

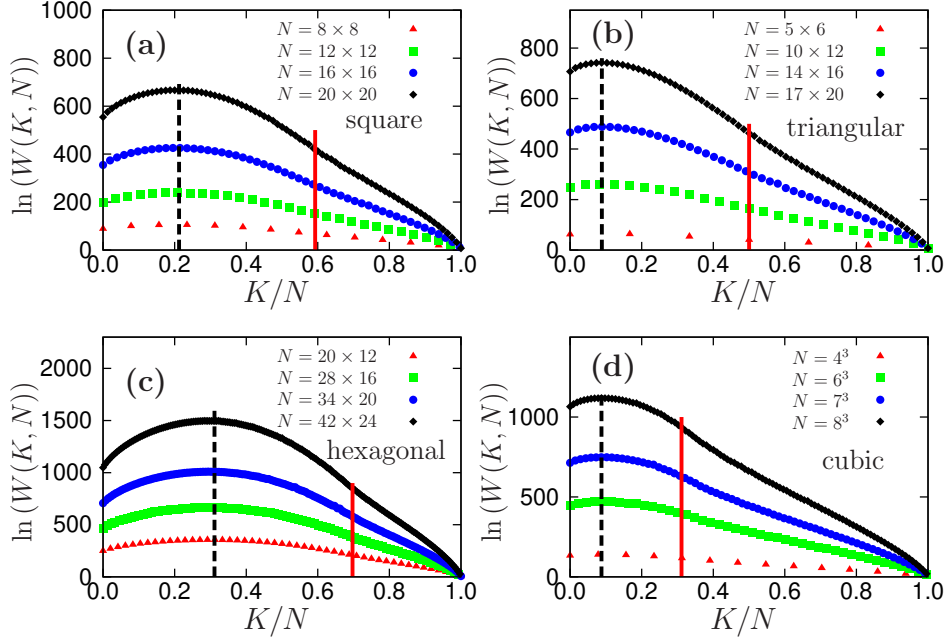


FIG. 5. Contributions to partition function $\ln W(K, N)$ (Eq.(7)) as a function of the connected-site fraction $p = K/N$ and different system sizes N and lattices: (a) square; (b) triangular; (c) hexagonal; (d) cubic. Vertical red lines indicate the corresponding site-percolation thresholds.

of small, finite clusters. This is confirmed by the average cluster size $\langle S \rangle$ shown in Fig.6, which are really small (for triangular and cubic lattices most of clusters contain just one spin) and tends to a constant as $N \rightarrow \infty$.

The total number of ground states is given by the sum over all possible numbers of connected bonds K

$$W(N) = \sum_{K=0}^N W(K, N) \quad (8)$$

Using the numerical Monte-Carlo approach details in Ref.[24], we find that for all studied lattices (hexagonal, square, triangular, cubic), the ground state degeneracy grows exponentially with N

$$W(N) \sim e^{\alpha N} \quad (9)$$

with a lattice-dependent exponent α . This leads to a residual entropy per spin

$$\mathcal{S}_0(N) = \frac{\ln(W(N))}{\mathcal{N}} \quad (10)$$

where $\mathcal{N} = 2N + \frac{1}{2}zN$ is the total number of spins- $\frac{1}{2}$.

The results for $\mathcal{S}_0(N)$ vs. $1/N$ for different lattices are plotted in Fig. 7.

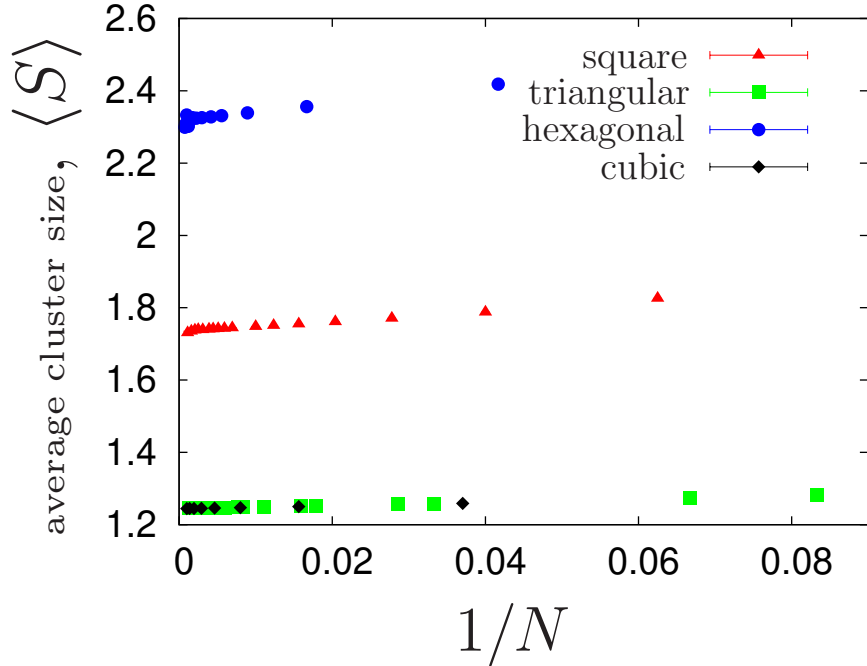


FIG. 6. Average cluster size $\langle S \rangle$ as a function of the $1/N$ for different lattices.

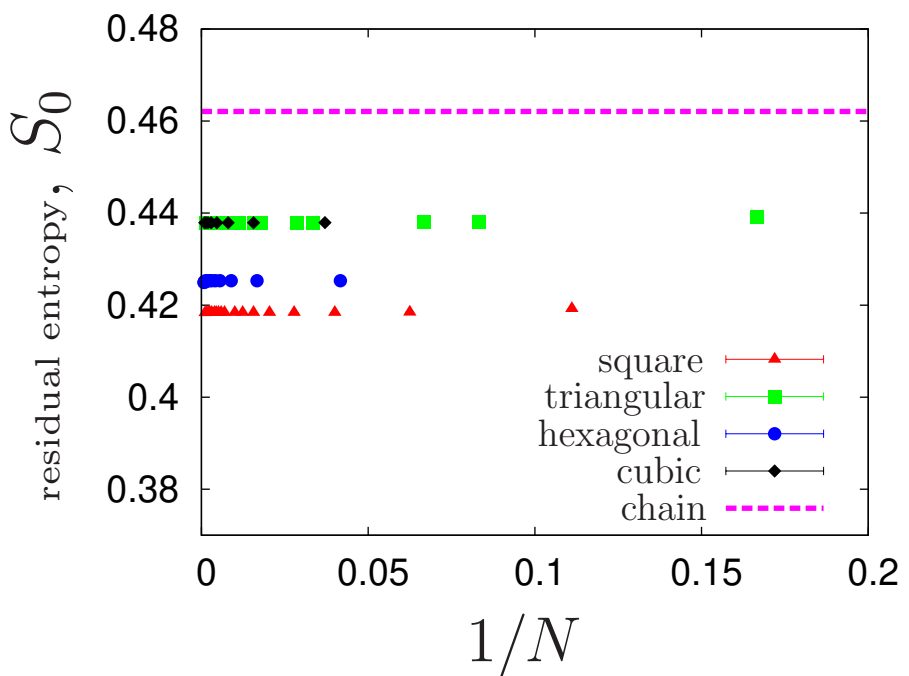


FIG. 7. Residual entropy $S_0(N)$ as a function of $1/N$ for the square, triangular, honeycomb and cubic lattices.

TABLE I. Residual entropy per spin, \mathcal{S}_0 , for diamond-decorated model, connected star model at the quantum critical point and connected star model in the MD phase

Lattice	Diamond-decorated	Critical point	MD phase
Chain ($z = 2$)	0.462	0.462	0.231
Hexagonal ($z = 3$)	0.402	0.425	0.297
Square ($z = 4$)	0.362	0.418	0.347
Triangular ($z = 6$)	0.314	0.438	0.416
Cubic ($z = 6$)	0.302	0.438	0.416

Figure 7 shows that $\mathcal{S}_0(N)$ converges to a finite thermodynamic limit for all lattices, which gives the thermodynamic values of the residual entropy

$$\mathcal{S}_0 = \frac{\alpha}{2 + \frac{z}{2}} \quad (11)$$

Table 1 lists these limiting values of \mathcal{S}_0 , alongside the residual entropies for diamond-decorated models [24] and for the monomer-dimer (MD) phase of the present model.

Table 1 reveals two key findings. First, the residual entropy for connected-star models is systematically higher than for diamond-decorated models across all lattices. Second, while the entropy of diamond-decorated models decreases with coordination number z , the residual entropy of connected-star models remains high (exceeding 60% of the maximal entropy $\ln 2$) and even increases slightly with z at the quantum critical point. This contrasts with the MD phase, where the residual entropy grows with z due to the increasing number of free bond spins - a trend that nearly saturates to the quantum critical point value for the cubic lattice.

B. Magnetization

For a macroscopically degenerate ground state manifold, the zero-temperature magnetization M is defined by an average over all ground states $|\psi_k\rangle$:

$$M^2 = \frac{1}{W} \sum_{k=1}^W \langle \psi_k | \mathbf{S}_{tot}^2 | \psi_k \rangle \quad (12)$$

where $\mathbf{S}_{tot} = \sum \mathbf{s}_i$ is the total spin operator and the averaging is performed over all W ground states $|\psi_k\rangle$. In the thermodynamic limit, this definition corresponds to the square

root of the long-range spin correlation $\langle \mathbf{s}_i \cdot \mathbf{s}_j \rangle$ ($|\mathbf{i} - \mathbf{j}| \rightarrow \infty$), averaged over the ground state manifold. For a pure ferromagnet with \mathcal{N} spins- $\frac{1}{2}$, Eq.(12) correctly reproduces the saturation magnetization per spin $m = \frac{M}{N} = \frac{1}{2}$.

We calculate m using the percolation mapping, following the approach of Ref.[24]. If a configuration ω_K contains only small clusters (the number of which is proportional to N), the total spin of each cluster is of order unity, and the magnetization per spin vanishes as $m \sim N^{-1/2}$. In contrast, if ω_K contains an infinite percolation cluster of weight P (i.e., a fraction P of all spins belong to a single connected cluster), then $m = P$.

According to percolation theory, an infinite cluster exists only above the site-percolation threshold p_c , growing as $P \sim (p - p_c)^\beta$ for $p > p_c$, with $\beta \simeq 0.14$ for 2D and $\beta \simeq 0.4$ for 3D lattices [31, 32]. Therefore, the presence of magnetic order depends on whether the typical value of $p = K/N$ in the ground state ensemble lies above p_c . As shown in Fig.5(a)-(d), the function $W(K, N)$ - and hence the statistical weight of configurations - peaks at values p_0 well below the corresponding p_c for all lattices. Consequently, configurations containing an infinite cluster are exponentially suppressed in the thermodynamic limit, and the ground-state magnetization must vanish.

This prediction is confirmed numerically in Fig. 8, where the magnetization per spin $m(N)$ scales as $N^{-1/2}$ for all studied lattices.

We now examine the full magnetization curve in an external magnetic field h at low temperature. In the ferromagnetic phase ($J_1 < 2J_2$), the magnetization behavior depends crucially on dimensionality. For three-dimensional lattices, robust long-range ferromagnetic order exists, leading to saturation magnetization $m = 1/2$ for an infinitesimal field. In two dimensions, however, the Mermin-Wagner theorem precludes long-range order at finite temperature, resulting in magnetization that increases rapidly as $m \sim h \exp(\text{const.}/T)$ before eventually saturating at $m = 1/2$.

Within the MD phase ($J_1 > 2J_2$), the free monomer spins on the lattice bonds produce a linear paramagnetic response at weak fields, $m \sim h/T$. With a further increase of the magnetic field, all monomer spins are polarized and the magnetization comes to a plateau at $m_0 = \frac{z}{2z+8}$ ($m_0 = 1/4$ for the square lattice). This plateau persists up to a critical field $h_c = J_1 - 2J_2$, which corresponds to the energy gap $E_F - E_0 = J_1 - 2J_2$ required to excite a composite spin from the singlet ($L = 0$) to the triplet ($L = 1$) state. For $h > h_c$, all composite spins are forced into the $L = 1$ state, and the system enters the fully polarized

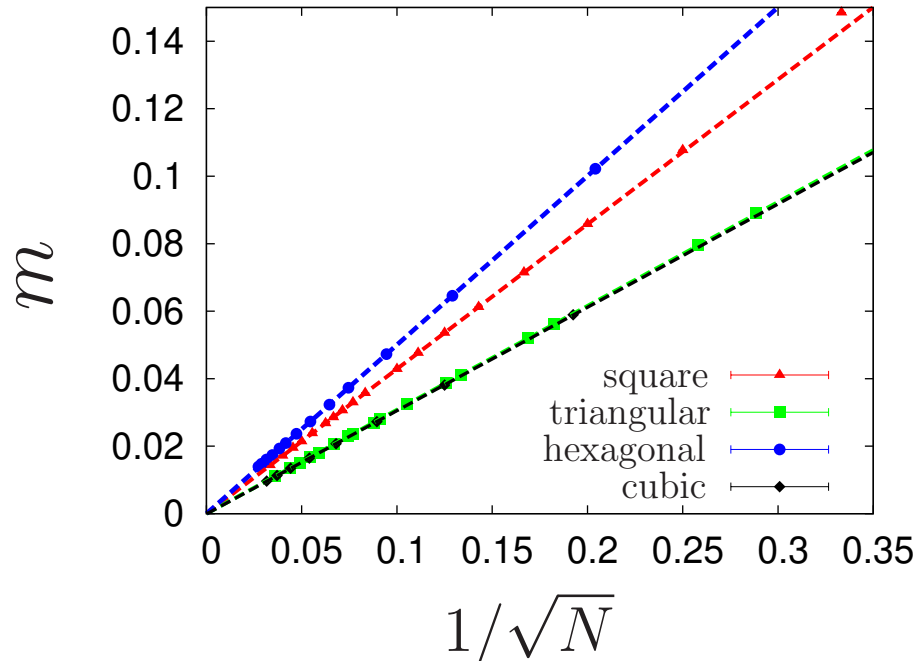


FIG. 8. Magnetization per spin as a function of $N^{-1/2}$ for square, honeycomb, triangular and cubic lattices. The linear behavior confirms $m \sim N^{-1/2}$ at large N .

ferromagnetic phase with saturation magnetization $m = 1/2$.

At the quantum critical point ($J_1 = 2J_2$), the fully polarized state belongs to the ground state manifold at $h = 0$. While an infinitesimal field would select this state at strictly zero temperature, the behavior at low but finite temperature T is governed by a competition between entropic and energetic contributions. The partition function is dominated by two terms, $Z \approx Z_1 + Z_2$. The first term Z_1 originates from the exponentially numerous configurations with a fraction $p \simeq p_0$ of triplet sites below the percolation threshold p_c :

$$Z_1 \sim \exp \left(\mathcal{S}_0 \mathcal{N} + \frac{h \mathcal{N}}{2T} - \frac{h N (1-p_0)}{T} \right) \quad (13)$$

The second term Z_2 comes from the much fewer nearly polarized states above the percolation threshold, which have lower Zeeman energy. Therefore, the second term can be approximated as

$$Z_2 \sim \exp \left(\frac{h \mathcal{N}}{2T} \right) \quad (14)$$

Comparing Z_1 and Z_2 , we find that Z_1 dominates for $h \ll T$, whereas Z_2 prevails in the opposite limit $h \gg T$. This means that for $h \ll T$, the system behaves as paramagnet with

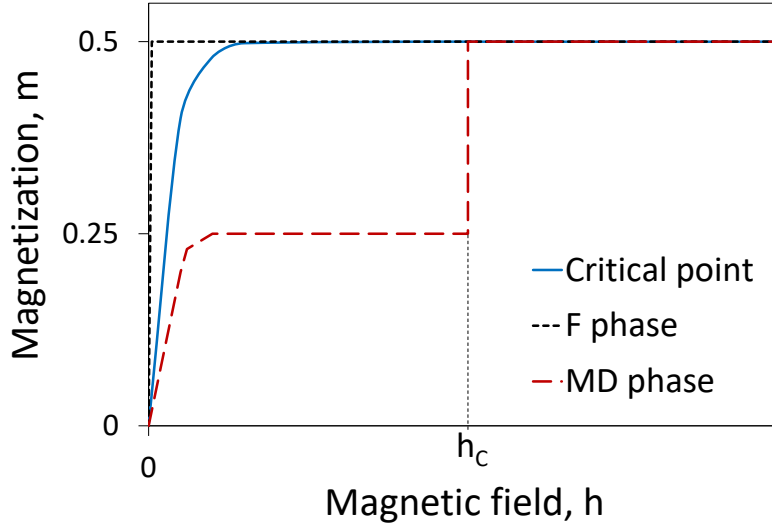


FIG. 9. Schematic magnetization curves in the low-temperature limit for the ferromagnetic phase (black long-dashed line), the MD phase (red dashed line), and at the quantum critical point (blue solid line). In the MD phase and at the quantum critical point for $h \ll T$, the slope is proportional to $1/T$.

$m \sim \frac{h}{T}$. When $h \gg T$, the system behaves as ferromagnet, which means the saturation of magnetization $m = \frac{1}{2}$.

All these results are summarized and schematically shown in Fig.9.

C. Excitation spectrum and specific heat

The one-magnon excitation spectrum of the connected stars model on the square lattice can be calculated exactly. It consists of two flat bands with energies $E_0 = 0$ (the ground-state band) and $E_1 = 2$, along with two dispersive branches

$$E_{2,3}(\mathbf{k}) = 2 \pm 2\sqrt{1 - \frac{1}{4}(2 - \cos k_x - \cos k_y)} \quad (15)$$

Near $k_x = k_y = 0$ the lower branch behaves as

$$E_2(\mathbf{k}) = \frac{1}{8}\mathbf{k}^2 \quad (16)$$

indicating a gapless quadratic dispersion similar to that of a conventional ferromagnet. Consequently, on a finite system of linear size n , the finite-size gap scales as $\sim n^{-2}$ or N^{-1} for $N = n^2$ sites. Analogous calculations for other lattices (triangular, hexagonal, cubic) likewise yield a gapless, quadratic low-energy spectrum $E(\mathbf{k}) \sim \mathbf{k}^2$.

Despite this gapless dispersion in the thermodynamic limit, the dominant ground state configurations consist almost entirely of small, disconnected ferromagnetic clusters. As established in Sec.IIb, the statistical weight of configurations containing an infinite (spanning) ferromagnetic cluster is exponentially suppressed. The typical cluster size remains finite as $N \rightarrow \infty$, implying that most local excitations are gapped.

This leads to a marked separation of energy scales in the thermodynamics. Contributions from the gapless magnons (16) are weighted by the exponentially small probability of being in a configuration that supports such long-range excitations. For example, the low-temperature specific heat is governed by a competition between two distinct contributions: one from the gapless modes, $C_1 \sim T^{d/2} e^{-S_0 \mathcal{N}}$ (where d is the lattice dimension and S_0 is the residual entropy per spin), and another from the gapped excitations of the dominant finite clusters, $C_2 \sim (\Delta/T)^2 e^{-\Delta/T}$ (with Δ is a typical cluster gap).

Comparing these terms shows that C_1 dominates only at extremely low temperatures, $T < \Delta/(S_0 \mathcal{N})$. In the thermodynamic limit $N \rightarrow \infty$, this temperature scale vanishes. Therefore, despite the formal presence of gapless excitations in the spectrum, the low-temperature thermodynamics of the system is effectively governed by gapped, local excitations, resembling that of a paramagnet with a finite energy gap.

III. DISTORTED STAR MODEL ON 2D AND 3D LATTICES

We now extend the connected-star model to include a structural distortion, where each monomer spin is coupled to the two spins of a neighboring dimer via two distinct exchange integrals, J_2 and J_3 (see Fig. 10). To realize macroscopic ground-state degeneracy, the condition for each triangular plaquette - formed by two dimer spins and one monomer spin - must be satisfied: its ground-state manifold must include both a quartet ($S = \frac{3}{2}$) and one of its two doublets states ($S = \frac{1}{2}$). For a single triangle, this requires

$$\frac{1}{J_1} + \frac{1}{J_2} + \frac{1}{J_3} = 0 \quad (17)$$

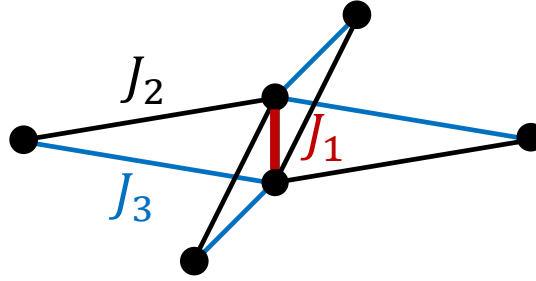


FIG. 10. Example of distorted star. Exchanges between dimer spins J_1 are shown by red lines, the exchanges of monomer spins with dimer spins, J_2 and J_3 , are shown by black and blue lines.

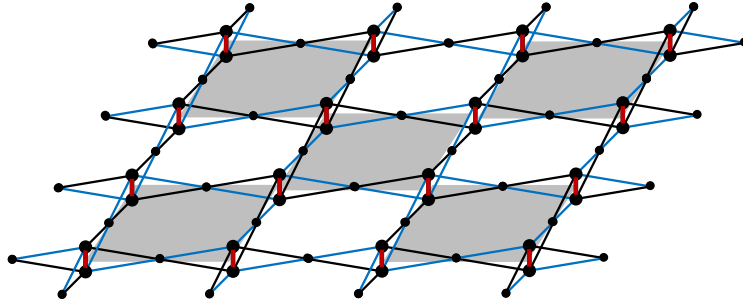


FIG. 11. Distorted star model on square lattice. Shaded squares denote trapping cells.

For the star containing z edge-shared triangles, the conditions (17) transforms to

$$\frac{z}{J_1} + \frac{1}{J_2} + \frac{1}{J_3} = 0 \quad (18)$$

Throughout, we assume that black exchanges $J_2 < 0$ is ferromagnetic and $|J_2| > |J_3|$.

Multiple inequivalent distributions of J_2 and J_3 bonds are possible on a given lattice. To compute the ground-state degeneracy for a specific arrangement, we apply the method proposed in Ref. [24]: set $J_1 = J_3 = 0$, leaving only the ferromagnetic J_2 bonds. The system then effectively decouples into numerous independent ferromagnetic clusters. The product of the multiplet degeneracies of all clusters gives the total ground-state degeneracy, which remains exact for any J_1 and J_3 satisfying Eq.18.

For the square lattice, the distribution shown in Fig.11 maximizes the degeneracy. In this configuration, the J_2 (black) bonds form disjoint squares, each enclosing eight spins- $\frac{1}{2}$. An isolated square has a ferromagnetic ground state degeneracy of $2S + 1 = 9$ (for total spin $S = 4$). Since the squares are decoupled when $J_1 = J_3 = 0$, the total degeneracy

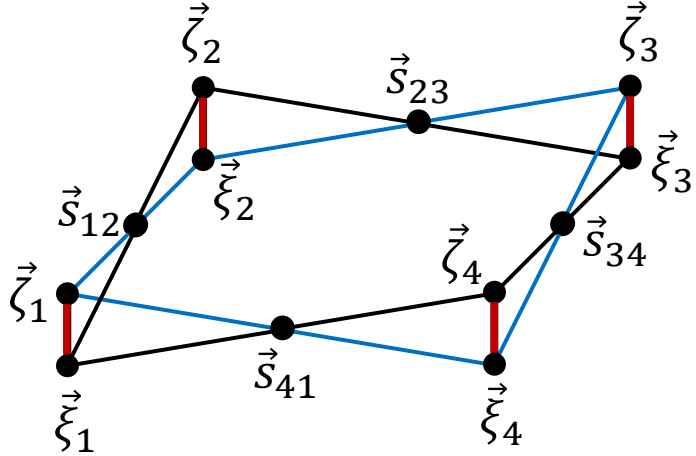


FIG. 12. Trapping cell for distorted-star model.

is $W = 9^{N/8}$, where N is the number of lattice sites (stars). The corresponding residual entropy per spin is $S_0 = \frac{1}{8} \ln 9 \simeq 0.275$.

This result can be verified by constructing the exact localized multi-magnon ground states within a single square trapping cell, shown in Fig.12. The one-magnon state is

$$\hat{\varphi}_1 = (s_{12}^- + s_{23}^- + s_{34}^- + s_{41}^- + \sigma_1^- + \sigma_2^- + \sigma_3^- + \sigma_4^-) |F\rangle \quad (19)$$

where

$$\sigma_i^- = \frac{\xi_i^- + J\zeta_i^-}{1 + J} \quad (20)$$

and ξ_i^- , ζ_i^- are lowering operators of dimer spins and $J = J_3/J_2$ (J_1 is defined by Eq.(18)).

Higher multi-magnon states are generated recursively:

$$\hat{\varphi}_2 = \hat{\varphi}_1^2 - \sum \sigma_i^{-2} |F\rangle \quad (21)$$

and, generally, k -magnon localized state in the trapping cell ($k = 1, 2, \dots, 8$) is

$$\hat{\varphi}_k = \hat{\varphi}_1^{k-2} \left(\hat{\varphi}_1^2 - \frac{k(k-1)}{2} \sum \sigma_i^{-2} \right) |F\rangle \quad (22)$$

so that, the maximal possible eight-magnon state is

$$\hat{\varphi}_8 = s_{12}^- s_{23}^- s_{34}^- s_{41}^- \sigma_1^- \sigma_2^- \sigma_3^- \sigma_4^- |F\rangle \quad (23)$$

Thus, a single square supports nine exact states (with magnon numbers $0, 1, 2, \dots, 8$).

Crucially, the product of exact localized magnon states from neighboring squares is not itself an exact eigenstate of the full Hamiltonian. However, as shown in [24], an exact eigenstate can be formed by adding a specific correction term:

$$\hat{\varphi}_k^{(1)} \hat{\varphi}_m^{(2)} |F\rangle + 2J\xi_{12}^- \zeta_{12}^- \hat{\varphi}_{k-1}^{(1)} \hat{\varphi}_{m-1}^{(2)} |F\rangle \quad (24)$$

where ξ_{12}^- , ζ_{12}^- are spin operators on the shared dimer between two neighboring trapping cells 1 and 2. This construction demonstrates that there is no hard-core repulsion preventing magnons from occupying adjacent trapping cells; the exact many-body ground states are products of the localized multi-magnon states, appropriately corrected along shared dimers. Consequently, the total ground-state manifold is equivalent to that of $\frac{N}{2}$ non-interacting spins of length $s = 4$, confirming $W = 9^{N/8}$ and the corresponding residual entropy. Therefore, at low temperatures the system mimics a paramagnetic crystal of non-interacting spins $s = 4$.

A similar construction for the cubic lattice yields disjoint cubes formed by black J_2 bonds, each containing 20 spins-1/2 and a ferromagnetic degeneracy of 21. This gives the ground state degeneracy of the total system $W = 21^{N/20}$, which produces the residual entropy $S_0 = \frac{1}{20} \ln 21 \simeq 0.152$.

Both values are significantly lower than the residual entropies of the ideal (undistorted) star models (see Table 1), indicating that distortion reduces the ground state degeneracy. These analytical results are confirmed by exact diagonalization of finite systems.

As noted previously, in the limit $J_1 = J_3 = 0$, the system decouples into non-interacting ferromagnetic clusters (trapping cells), each containing eight spins $\frac{1}{2}$. The lowest excitation above the macroscopically degenerate ground state in this limit corresponds to the first excited state of an individual cluster, which is finite. Consequently, the spectrum is gapped at $J_1 = J_3 = 0$.

The full one-magnon excitation spectrum for the distorted model, calculated with general couplings satisfying Eq. (18), remains gapped for all allowed values of J_1, J_2, J_3 . Together, these results confirm the existence of a finite energy gap ΔE in the spectrum of the distorted-star model. Consequently, at temperatures $T < \Delta E$, the low-field magnetization and susceptibility correspond to a paramagnet of non-interacting spins $s = 4$: $m = \frac{11}{3} \frac{h}{T}$ and $\chi = \frac{11}{3} T$ for $h \ll T$.

We have focused here on a specific, optimal arrangement of exchanges J_2 and J_3 for the square lattice. The construction generalizes directly to other lattices, subject only to

the constraint that every monomer spin connects to its neighboring dimer via two distinct exchanges satisfying Eq.(18). Different distributions of J_2 and J_3 will yield different, typically smaller, ground-state degeneracies.

IV. SUMMARY

In this work, we have explored a class of highly frustrated spin-1/2 Heisenberg models on two- and three-dimensional lattices constructed from connected star units, where each star comprises edge-sharing triangles, featuring antiferromagnetic couplings along shared edges and ferromagnetic couplings on the others. Our analysis reveals that these architectures support exceptionally high ground-state degeneracy and corresponding residual entropy.

For the ideal (undistorted) star model at the quantum critical point $J_1 = 2J_2$, we established an exact mapping of the ground state manifold onto a site percolation problem on the Lieb lattice. This powerful correspondence allowed us to calculate the exponential degeneracy $W(N) \sim e^{\alpha N}$ and the thermodynamic residual entropy \mathcal{S}_0 for square, triangular, honeycomb, and cubic lattices. The obtained entropy is not only systematically larger than that of related diamond-decorated lattices but also remarkably robust, maintaining a high value (exceeding 60% of the maximal value $\ln 2$) independent of the lattice coordination number z . Despite the formal presence of gapless, quadratic ferromagnetic excitations $E(k) \sim k^2$ in the one-magnon spectrum, the low-temperature thermodynamics is dominated by the exponentially numerous, gapped excitations of small, finite ferromagnetic clusters. Consequently, observables like the specific heat behave as in a gapped system, with the contribution from the gapless modes being exponentially suppressed by the large residual entropy. This reflects a remarkable fact: while the spectrum is gapless, the thermodynamic weight of the corresponding low-energy states is negligible in the thermodynamic limit. The zero-temperature magnetization vanishes as $m \sim N^{-1/2}$, confirming the absence of long-range order due to the statistical dominance of configurations fragmented below the geometric percolation threshold.

For the distorted star model, macroscopic degeneracy arises under the generalized condition $z/J_1 + 1/J_2 + 1/J_3 = 0$. In the optimal bond arrangement for the square lattice, this leads to a ground state manifold equivalent to a system of non-interacting high-spin clusters, yielding a degeneracy $W = 9^{N/8}$ and entropy $\mathcal{S}_0 = 0.275$. The construction generalizes

to three dimensions, giving $W = 21^{N/20}$ and $\mathcal{S}_0 = 0.152$ for the cubic lattice. While these values are lower than those for the ideal star model, the degeneracy remains exponential and the excitation spectrum is gapped, leading to conventional low-temperature paramagnetic behavior.

In summary, we have shown that the architecture of connected-star lattices provides a design principle for quantum magnets with high residual entropy. The macroscopic degeneracy at quantum critical point identifies these systems as promising candidates for magnetocaloric cooling at ultra-low temperatures and as ‘entropic levers’ for quantum thermal machines. Our results establish a framework for engineering high-entropy magnetic materials for low-temperature applications.

[1] H. T. Diep *et al.*, *Frustrated spin systems* (World scientific, 2013).

[2] H. T. Diep, Frustrated spin systems: history of the emergence of a modern physics, *Comptes Rendus. Physique* **26**, 225 (2025).

[3] C. Lacroix, P. Mendels, and F. Mila, *Introduction to frustrated magnetism: materials, experiments, theory*, Vol. 164 (Springer Science & Business Media, 2011).

[4] J. Schulenburg, A. Honecker, J. Schnack, J. Richter, and H.-J. Schmidt, Macroscopic magnetization jumps due to independent magnons in frustrated quantum spin lattices, *Physical review letters* **88**, 167207 (2002).

[5] O. Derzhko, J. Richter, and M. Maksymenko, Strongly correlated flat-band systems: The route from heisenberg spins to hubbard electrons, *International Journal of Modern Physics B* **29**, 1530007 (2015).

[6] O. Derzhko, J. Richter, A. Honecker, and H.-J. Schmidt, Universal properties of highly frustrated quantum magnets in strong magnetic fields, *Low Temperature Physics* **33**, 745 (2007).

[7] M. Zhitomirsky and H. Tsunetsugu, Exact low-temperature behavior of a kagomé antiferromagnet at high fields, *Physical Review B* **70**, 100403 (2004).

[8] J. Strelčka, J. Richter, O. Derzhko, T. Verkholyak, and K. Karl'ová, Diversity of quantum ground states and quantum phase transitions of a spin-1/2 heisenberg octahedral chain, *Physical Review B* **95**, 224415 (2017).

[9] J. Richter, O. Derzhko, and J. Schulenburg, Magnetic-field induced spin-peierls instability in

strongly frustrated quantum spin lattices, *Physical review letters* **93**, 107206 (2004).

[10] J. Richter, O. Krupnitska, V. Baliha, T. Krokhmalskii, and O. Derzhko, Thermodynamic properties of $Ba_2CoSi_2O_6Cl_2$ in a strong magnetic field: Realization of flat-band physics in a highly frustrated quantum magnet, *Physical Review B* **97**, 024405 (2018).

[11] M. Zhitomirsky, Enhanced magnetocaloric effect in frustrated magnets, *Physical Review B* **67**, 104421 (2003).

[12] M. Zhitomirsky and A. Honecker, Magnetocaloric effect in one-dimensional antiferromagnets, *Journal of Statistical Mechanics: Theory and Experiment* **2004**, P07012 (2004).

[13] O. Derzhko and J. Richter, Finite low-temperature entropy of some strongly frustrated quantum spin lattices in the vicinity of the saturation field, *Physical Review B* **70**, 104415 (2004).

[14] V. Y. Krivnov, D. V. Dmitriev, S. Nishimoto, S.-L. Drechsler, and J. Richter, Delta chain with ferromagnetic and antiferromagnetic interactions at the critical point, *Phys. Rev. B* **90**, 014441 (2014).

[15] D. V. Dmitriev, V. Y. Krivnov, J. Richter, and J. Schnack, Thermodynamics of a delta chain with ferromagnetic and antiferromagnetic interactions, *Physical Review B* **99**, 094410 (2019).

[16] D. V. Dmitriev, V. Y. Krivnov, J. Schnack, and J. Richter, Exact magnetic properties for classical delta-chains with ferromagnetic and antiferromagnetic interactions in applied magnetic field, *Physical Review B* **101**, 054427 (2020).

[17] D. V. Dmitriev and V. Y. Krivnov, Delta chain with anisotropic ferromagnetic and antiferromagnetic interactions, *Physical Review B* **92**, 184422 (2015).

[18] D. V. Dmitriev and V. Y. Krivnov, Ferrimagnetism in delta chain with anisotropic ferromagnetic and antiferromagnetic interactions, *Journal of Physics: Condensed Matter* **28**, 506002 (2016).

[19] D. V. Dmitriev and V. Y. Krivnov, Two-dimensional spin models with macroscopic degeneracy, *Journal of Physics: Condensed Matter* **33**, 435802 (2021).

[20] Y.-H. Ma, S.-H. Su, and C.-P. Sun, Quantum thermodynamic cycle with quantum phase transition, *Phys. Rev. E* **96**, 022143 (2017).

[21] C. Purkait and A. Biswas, Performance of heisenberg-coupled spins as quantum stirling heat machine near quantum critical point, *Physics Letters A* **442**, 128180 (2022).

[22] B. Castorene, F. J. Peña, A. Norambuena, S. E. Ulloa, C. Araya, and P. Vargas, Effects of magnetic anisotropy on three-qubit antiferromagnetic thermal machines, *Physical Review E*

110, 044135 (2024).

[23] D. V. Dmitriev and V. Y. Krivnov, Macroscopic degeneracy of the ground state in the frustrated heisenberg diamond chain, *Physical Review B* **111**, 064427 (2025).

[24] D. V. Dmitriev, V. Y. Krivnov, and O. A. Vasilyev, Macroscopic ground state degeneracy of the heisenberg model with ferromagnetic and antiferromagnetic interactions on diamond-decorated lattices, *Phys. Rev. B* **112**, 094426 (2025).

[25] M. Fujihala, H. Koorikawa, S. Mitsuda, M. Hagiwara, H. Morodomi, T. Kawae, A. Matsuo, and K. Kindo, Spin-liquid ground state in the spin 1/2 distorted diamond chain compound $K_3Cu_3AlO_2(SO_4)_4$, *Journal of the Physical Society of Japan* **84**, 073702 (2015).

[26] G. S. Murugan, J. Khatua, S. Kim, E. Mun, K. R. Babu, H.-S. Kim, C.-L. Huang, R. Kalaivanan, U. R. Kumar, I. P. Muthuselvam, W. T. Chen, S. Krishnamoorthi, K.-Y. Choi, and R. Sankar, Spin dynamics and 1/3 magnetization plateau in the coupled distorted diamond chain compound $K_2Cu_3(MoO_4)_4$, *Phys. Rev. B* **111**, 144420 (2025).

[27] K. Takano, K. Kubo, and H. Sakamoto, Ground states with cluster structures in a frustrated heisenberg chain, *Journal of Physics: Condensed Matter* **8**, 6405 (1996).

[28] K. Morita and N. Shibata, Exact nonmagnetic ground state and residual entropy of $s=1/2$ heisenberg diamond spin lattices, *Journal of the Physical Society of Japan* **85**, 033705 (2016).

[29] Y. Hirose, A. Oguchi, and Y. Fukumoto, Exact realization of a quantum-dimer model in heisenberg antiferromagnets on a diamond-like decorated lattice, *Journal of the Physical Society of Japan* **85**, 094002 (2016).

[30] N. Caci, K. Karl'ová, T. Verkholyak, J. Strečka, S. Wessel, and A. Honecker, Phases of the spin-1/2 heisenberg antiferromagnet on the diamond-decorated square lattice in a magnetic field, *Physical Review B* **107**, 115143 (2023).

[31] A. A. Saberi, Recent advances in percolation theory and its applications, *Physics Reports* **578**, 1 (2015).

[32] A. Sur, J. L. Lebowitz, J. Marro, M. H. Kalos, and S. Kirkpatrick, Monte carlo studies of percolation phenomena for a simple cubic lattice, *J Stat Phys* **15**, 345 (1976).